Date:. 21 June 2019
EIC Detector R&D Progress Report and Proposal

Project ID:	eRD21
Project Name:	EIC Background Studies and the Impact on the Interaction Region and Detector Design
Period Reported:	1 Oct 2018 – 30 Sept 2019
Project Leaders:	Latifa Elouadrhiri and Charles Hyde
Contact Person:	Latifa Elouadrhiri `latifa@jlab.org`

Project Personnel: (project members in red receive (or are proposed to receive) support from eRD21 funds for their contributions to the project)
Vitaly Baturin (Old Dominion University)
Pavel Degtiarenko (Thomas Jefferson National Accelerator Facility)
Latifa Elouadrhiri (Thomas Jefferson National Accelerator Facility)
Yulia Furletova (Thomas Jefferson National Accelerator Facility)
Charles Hyde (Old Dominion University)
Kyungseon Joo (University of Connecticut)
Andrey Kim (University of Connecticut)
Alexander Kiselev ((Brookhaven National Laboratory)
Vasiliy Morozov (Thomas Jefferson National Accelerator Facility)
Amethyst Maps (ODU)
Nikolay Markov (University of Connecticut)
Christoph Montag (Brookhaven National Laboratory)
Christine Ploen (Old Dominion University)
Marcy Stutzman (Thomas Jefferson National Accelerator Facility)
Mike Sullivan (SLAC National Accelerator Laboratory)
Mark Wiseman (Thomas Jefferson National Accelerator Facility)

eRD21 Progress Report and FY2020 Renewal Proposal

Spokespersons: Latifa Elouadrhiri and Charles Hyde

21 June 2019

Abstract

We report on FY2019 (year 2) progress of the eRD21 project on background studies. We report on synchrotron radiation, beam-gas interactions, and total beam-beam interaction rates. For FY2020, we request funding for studies of detector occupancy from synchrotron radiation and upstream beam-gas interactions (particularly small-angle production), neutron production and subsequent thermalization from beam-gas interactions and beam-loss at collimators, and a novel luminosity monitor based on optical transition radiation.

Contents

1 Achievements and ongoing work in FY2019

In the past year, the JLEIC baseline design has been upgraded to ion momenta $P_A/Z = 200$ GeV/c to achieve *ep* CM energies of 100 GeV The Interaction Region (IR) layout and optics remain essentially the same, as illustrated in Fig. 1.

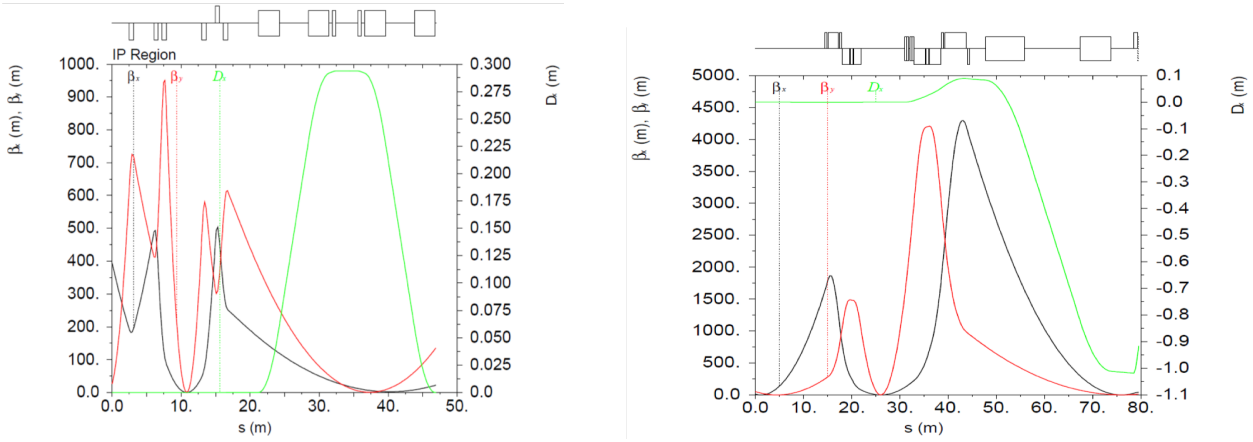

Fig. 1: Baseline JLEIC IR layout and optics. **Left:** Electron optics, with the Interaction Point (IP) at $s \approx 11$ m and the downstream Compton polarimeter IP at the high dispersion point region near $s \approx 34$ m. **Right:** Ion optics, the IP is at $s \approx 26$ m and a downstream secondary high-dispersion focus at $s \approx 75$ m.

The beam pipe design has been revised, to maximize residual gas conductance and minimize RF heating (Fig. 2).

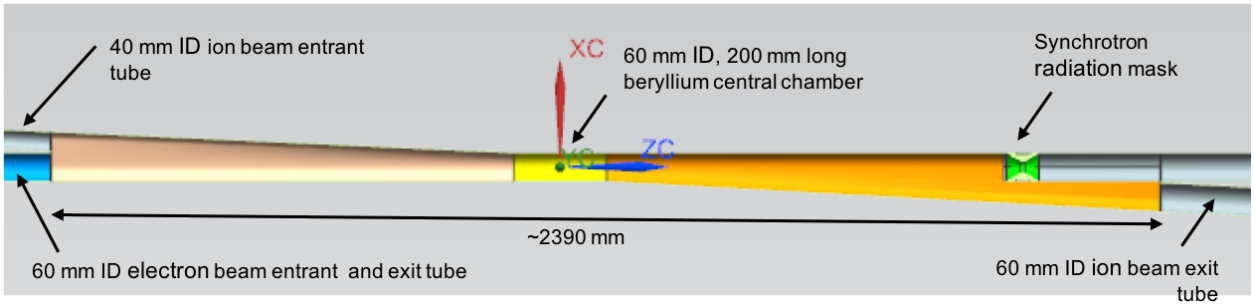

Fig. 2: JLEIC IR beam pipe, with 50 mrad horizontal crossing angle. Electrons are travelling along the $-z$ axis, with a 1.2 cm radius synchrotron mask on the electron beam-line at $z = 1$ m.

1.1 Vacuum Studies: M. Stutzman, lead

The new interaction region geometry has been incorporated in the Molflow+ vacuum model. Pumps are located between the IR volume and the cryomodules, as well as perfect pumping at the far extents of the modelled region at electron-line positions of +14.17 m & −10.48 m and ion-line positions −17.70 m & +22.00 cm. The pump locations are listed in Table 1. The pressure within the interaction region, assuming outgassing rates typical for stainless steel, is in the 10^{-10} Torr

range. Other materials are also being considered: vacuum materials such as copper, aluminum, and beryllium should provide similar if not lower outgassing rates. The pressure distribution along the electron beam-line is plotted in Fig. 3. The 3-D results for the full IR beam pipe are illustrated in Fig. 4.

Pump	Upstream position (m)	Speed (litre/sec)	Downstream position (m)	Speed (litre/sec)
Electron line	+1.50	800	−1.50	550
Ion Line	−1.35	500	+1.45	800

Table 1: Specifications of IP vacuum pumping.

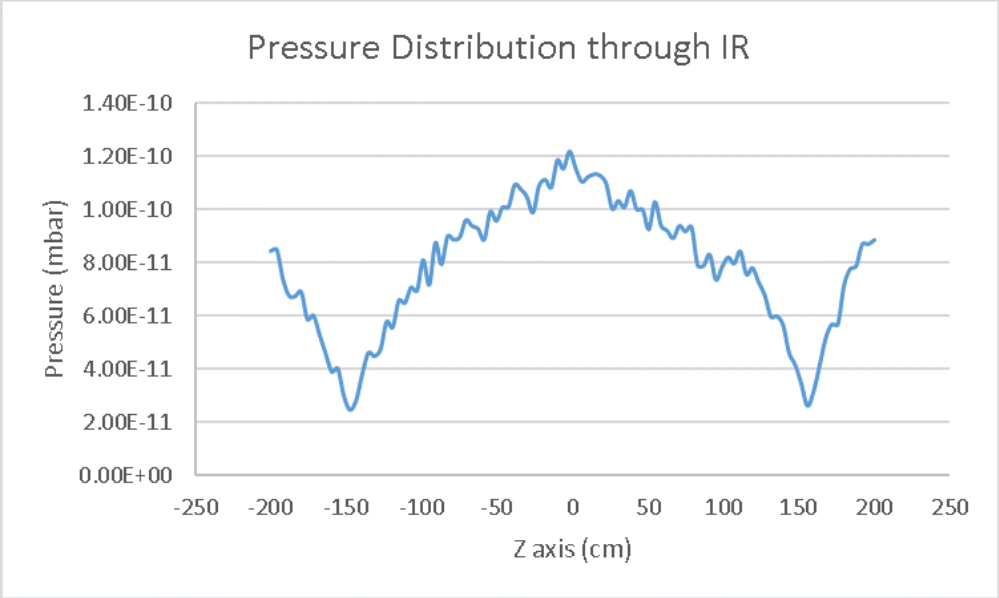

Fig. 3: Pressure distribution along electron beam line. Electrons enter at $z = 200$ cm, travelling in $-z$ direction.

The synchrotron radiation collimator position is 1 meter upstream in the electron line, and has a radius of 12 mm. The collimator does affect the pumping conductance, but the two beamlines share the central volume close to the collimator, minimizing the vacuum disruption in the system caused by the collimator constriction. Continuing work will involve adding the cold bore quadrupoles to the beamline and estimating both the pumping due to the cold bore and the saturation time before the cold bore magnets become saturated with gas. Improvements in the model will include improving the central chamber to more accurately model the pipe geometry, and considering other collimator locations which might reduce impedance induced heating.

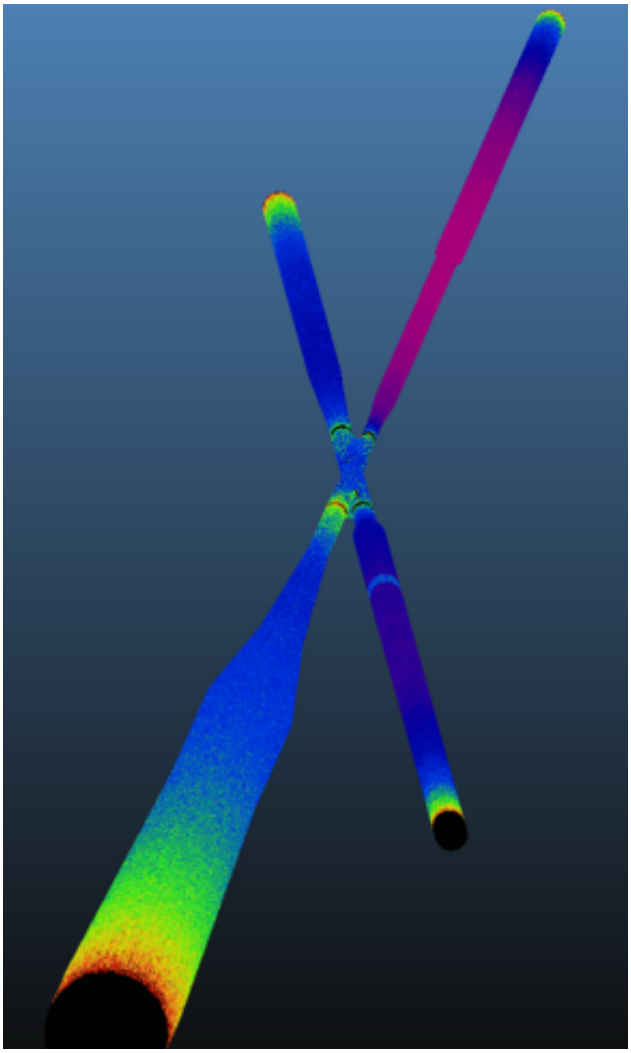

Fig. 4: Pressure profile in the electron and ion branches of the IR beampipe. Electrons enter from lower right and ions enter from upper right. The color scale (top) is in mbar (0.75 Torr). The upstream ion line has the highest pressure (magenta) at 10^{-9} Torr. The dark blue regions (including the IP) are 10^{-10} Torr. The pump locations near the IP are clearly visible, with pressure on the ion line dropping below 10^{-11} Torr.

1.2 Synchrotron Radiation: M. Sullivan, V. Baturin, C. Ploen, A. Kim

Dr. Vitaly Baturin started at ODU at the end of March 2019. The SYNRAD code has been ported to ODU/JLab. This is a semi-analytic code that generates the synchrotron power flux by scanning through the beam phase space as the electrons propagate through the magnetic elements. Each magnet is divided into four discrete longitudinal segments. Over each segment a beam electron is approximated at constant (x, y) but variable (x', y'). This defines a synchrotron "ray". We have now added a generator that takes the power flux from each ray, and generates a normalized ensemble of photons, with the energy distribution defined by the critical energy corresponding to the local magnetic field. The photon spectra are illustrated in Fig. 5. These spectra include the electron phase space and the beam-halo model from PEP-II.

Doctoral student Christine Ploen returned to the eRD21 project in May 2019. She has constructed a GEANT4 model of the electron beam pipe and the first two layers of a Si vertex tracker, illustrated in Fig. 6. The output from SYNRAD has been converted into a Lund-format file of photons passing the mask 1.0 m upstream of the IP. This photon distribution will be input to the GEANT4 model to obtain the power deposition in the central chamber and in the Si Tracker,

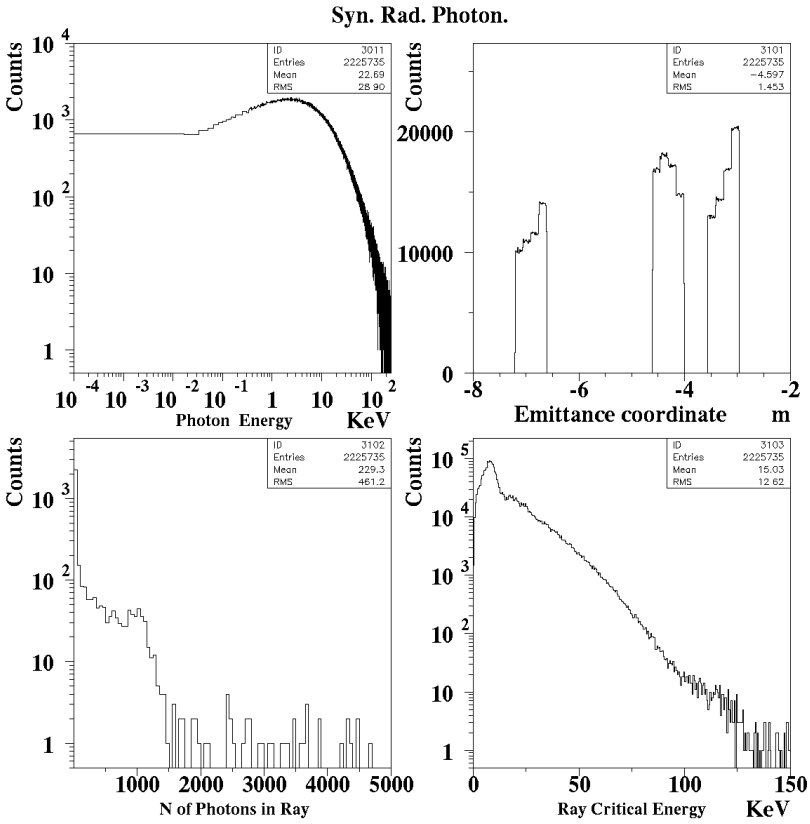

Fig. 5: SYNRAD Flux: **Top-left:** Synchrotron radiation (SR) photon energy distribution for all radiated photons (KeV). **Top-right**: Longitudinal-vertex distribution of generated photons: $s = -z$ in meters. The four discrete SYNRAD segments of each of the three FFQ magnets are evident. **Bottom-left:** Number of SR photons per bunch of 10^{10} electrons, generated in each of the 12 quad segments; **Bottom-right:** Distribution of critical energies for all SR rays in SYNRAD. The long tail is mostly due to halo electrons. The peak around 10 KeV is dominated by the primary beam.

as well as the per-beam-crossing occupancy of the Si tracker. After these initial studies, we will integrate the synchrotron flux simulations into the full scale detector simulations.

1.3 Beam-Gas Interactions: L. Elouadrhiri, A. Kiselev, C. Ploen

Our studies reported previously focused on the beam-gas interactions with the vacuum "bump" around the IP and prompt neutrons generated by beam-beam interactions. We validated the beam-gas studies by modelling the HERA-II backgrounds. A manuscript is in preparation. Neutron fluxes were calculated througout the BEAST detector, based on beam-beam collisions. Future work will examine beam gas interactions over a much greater range of the beam line, and start considering how neutrons thermalize in their interactions with the beam line elements and the tunnel walls.

1.4 Total Beam-Beam Interaction Rates: Charles Hyde

The total electron-ion hadronic production cross section is dominated by quasi-real photo-production. This can be written as (ignoring the crossing angle and integrating over the electron scattering azimuthal angle):

$$\begin{aligned} \frac{d^2\sigma(e,e')}{dW^2dQ^2} &= \frac{d^2\Gamma}{dW^2dQ^2}\sigma_\gamma \\ \frac{d^2\Gamma}{dW^2dQ^2} &= \frac{\alpha}{2\pi}\frac{W^2-M^2}{(s-M^2)^2Q^2}\frac{1}{1-\epsilon}, \end{aligned} \tag{1}$$

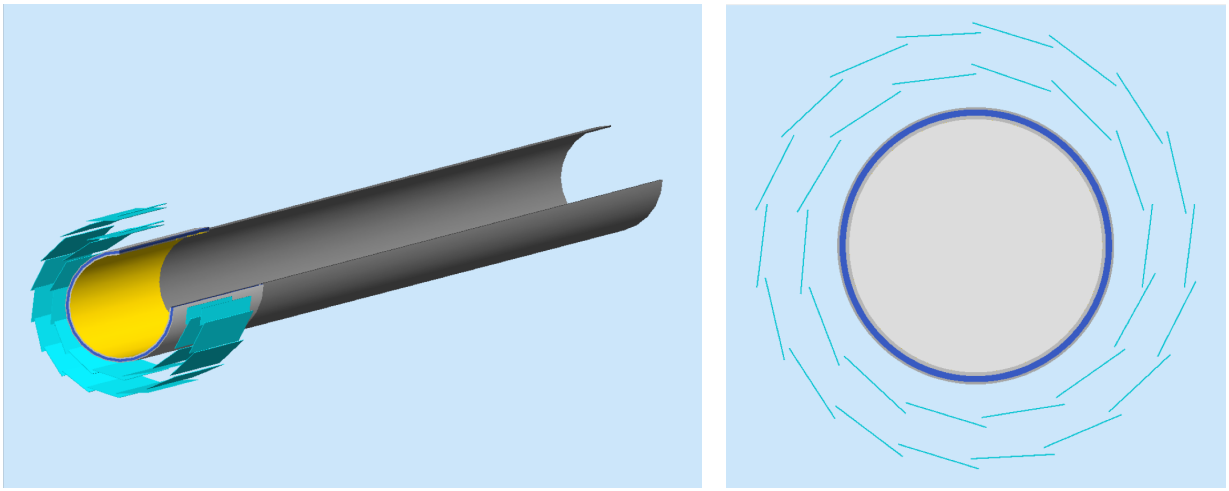

Fig. 6: GEANT4 model of electron beam pipe with two layers of Si vertex tracking (ion beam pipe not yet included). **Left:** Longitudinal view. **Right:** Transverse view. The central chamber is 20 cm long with a 6 cm inner diameter. From inside to out, the chamber wall is 4 μm Au, 0.83 mm Be, 1.48 mm H_2O, and 0.53 mm Be. These specifications are copied from BABAR [1]. The vacuum pressure is 10^{-10} Torr. The most realistic gas composition is under discussion.

Note that for $W^2 - M^2 > 0$, Q^2 is strictly positive:

$$\begin{aligned} Q^2 &= 2kk'(1-\cos\theta_e) + Q^2(0^\circ) \\ Q^2(0^\circ) &= m_e^2\left[\frac{(k-k')^2}{kk'} + \mathcal{O}(m_e^2/(kk')\right] = m_e^2\frac{(W^2-M^2)^2}{(s-M^2)(s-W^2)} + \mathcal{O}(m_e^4), \end{aligned} \tag{2}$$

with k, k' the incident and scattered electron energies. Neglecting terms of order Q^2/W^2

$$\begin{aligned} \frac{1}{1-\epsilon} &\to 1 - \frac{2}{y} + \frac{2}{y^2} \qquad y \to \frac{W^2-M^2}{s-M^2} \\ \frac{d^2\Gamma}{dW^2dQ^2} &\to \frac{\alpha}{2\pi}\frac{1}{Q^2}\frac{1}{W^2-M^2}\left[1 - \frac{W^2-M^2}{s-M^2} + \frac{1}{2}\left(\frac{W^2-M^2}{s-M^2}\right)^2\right] \end{aligned} \tag{3}$$

Integrating over Q^2, we obtain a simple $\log\left[(Q^2_{\rm Max})/Q^2(0^\circ)\right]$ dependence, provided $Q^2_{\rm Max} \ll W^2$ and $Q^2_{\rm Max}$ is less than the scale of Q^2-dependence in σ_γ. If we are interested in tagging individual photo-production events with the 0° electron tagger in the Compton polarimeter chicane, integrate over the tagger acceptance, which is in-principle W^2-dependent. A previous study by K.-J. Park showed that the JLEIC downstream optics has 100% acceptance up to 3 mrad for $k'/k > 10\%$.

The total inclusive and tagged rates can be expressed as

$$\begin{aligned} {\rm Rate} &= \mathcal{L}\int_{\rm Threshold}^{s} t^V\left(W^2, Q^2_{\rm Max}\right)\frac{dW^2}{W^2-M^2}\sigma_\gamma(W^2) \\ t^V\left(W^2, Q^2_{\rm Max}\right) &= \int^{Q^2_{\rm Max}}(W^2-M^2)\frac{d^2\Gamma}{dW^2dQ^2}dQ^2, \end{aligned} \tag{4}$$

where t^V is the equivalent effective radiator for quasi-real photons. In Fig. 7, we present a calculation of t^V, and the integrate inclusive and tagged rates.

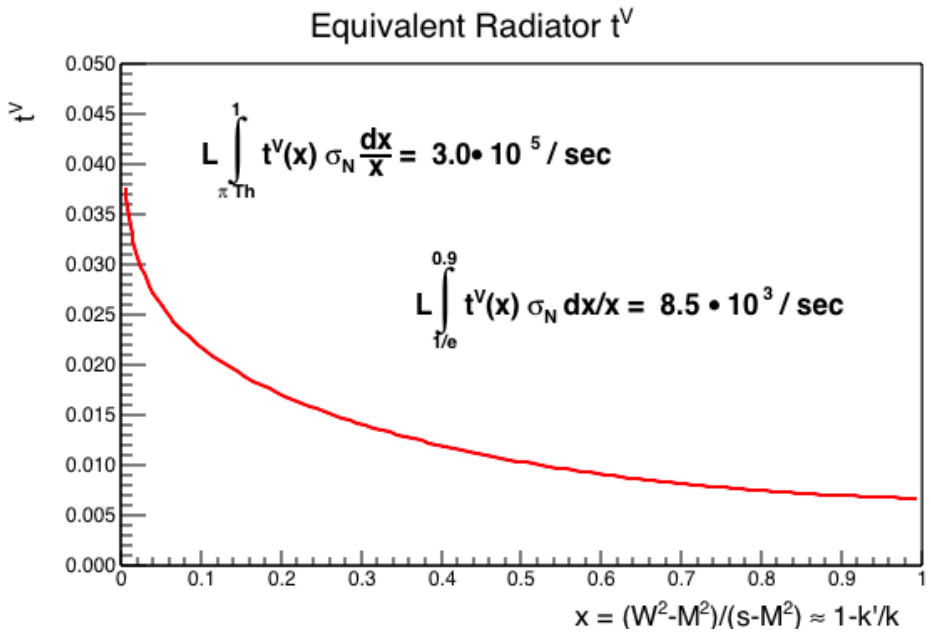

Fig. 7: Equivalent radiator t^V for quasi-real photo-production (Eq. 4). The calculation is for 3 GeV electrons incident on 200 GeV/c protons with the scattered electron angle integrated up to 3 mrad. Event rates are obtained with $\mathcal{L} = 10^{34}/\text{cm}^2/\text{sec}$ and a simple cross section model $\sigma_N = 100\mu\text{b}$ above pion threshold. The total inclusive hadro-production rate is $3 \cdot 10^5/\text{sec}$, and the tagging rate with a 0° acceptance $k'/k \in [1/e, 0.9]$ is $8.5 \cdot 10^3/\text{sec}$.

In our future work, we will improve the cross section model to include at least the Δ-resonance, and also compute the double longitudinal spin asymmetry A_{LL} to the inclusive rates, based on parameterizations of the integrand of the Gerasimov-Drell-Hearn Sum Rule. We will also provide a simple estimate of the neutron production rate in nuclei, based on the Giant Dipole Resonance.

2 Proposal for FY2020

2.1 Beam-Gas Neutrons and Small Angle Tracks: L. Elouadrhiri lead

We will extend our previous studies to include beam-gas interactions over the entire straight sections surrounding the Interaction Region. Including the apertures of the beam-line magnetic elements, and the end-cap calorimeters, we will produce accurate estimates of small angle tracks emanating from far upstream, that can nonetheless provide significant background to detectors located close to the beams.

We will also model the production, propagation, and thermalization of neutrons throughout the ring. This is in-principle a subset of the basic beam-gas interaction study. However, with the expectation that thermal neutrons form essentially a gas that diffuses throughout the ring, this aspect requires special treatment. P. Degtiarenko has extensive experience validating various simulation-tools for neutron production and thermalization. We will first determine what combination of codes will be most effective. It is expected that all of the accelerator equipment in the tunnel (as well as the tunnel wall material) will strongly influence the propagation of neutrons. We will construct a simplified model including idealized tunnel walls, and a set of iron tubes along the

beam lines, approximating the total mass and distribution of magnets along the accelerator. V. Morozov and M. Wiseman have inventories of all JLEIC magnets, that will form the basis for the model.

2.2 Optical Transition Radiation Luminosity Monitor: Y. G. Sharabian, lead

We propose to investigate and test a new solution for a fast, reliable, and relatively simple luminosity monitor based on the use of Optical Transition Radiation (OTR) [2, 3]. We propose the construction and the testing of two versions, *i.e.* different types of radiators and light collection techniques, so as to evaluate their respective merits.

A relativistic charged particle generates Optical Transition Radiation emitted along its trajectory and also in the backward hemisphere. We plan to use only the backward OTR component, which has remarkable features that provide flexibility in choosing the detection topology at negligible background. The simplest OTR monitors are used to measure the intensity of the beam in high energy accelerators. For EIC luminosity monitoring, we need to detect a well known high-rate process. The limits on absolute and relative precision depend on background levels, acceptance and efficiency systematics, and the theory of the process. Key features of OTR relevant for a luminosity monitor include:

- It is an instantaneous process.
- The probability of photon emission in a single transition is about 2% (*i.e.* α) and is a weak function of electron energy, varying as $\sim \ln\gamma$, where γ is the Lorentz factor,
- The photons of backward OTR are emitted from the precise entry point of the electron trajectory into the medium.
- The angular dependence (and absolute flux per incident electron of backward OTR photons emitted by an ideal conductor is:

$$\frac{d^3N_\gamma(\mathbf{k}_\gamma)}{(d\omega/\omega)d\Omega_\gamma} = \left[\frac{\alpha}{\pi^2}\right] \frac{\beta^2\sin^2\theta_\gamma}{(1-\beta^2\cos^2\theta_\gamma)^2} = f(\omega,\theta_\gamma,\phi_\gamma) \tag{5}$$

  where $\omega = |\mathbf{k}_\gamma|$ is the energy of the emitted photon, and $(\theta_\gamma, \phi_\gamma)$ are the polar and azimuthal angles of the photon wave vector $\mathbf{k}_\gamma$ relative to the reflection direction, defined in Fig. 8.

- Insensitive to neutral and low energy charged particles
- Target/radiator can be arbitrarily thin ($>> 1/k_\gamma$), and radiation hard.

The OTR optical flux (Eq. 5) angular distribution is plotted for several incident electron energies in Fig. 9;

2.3 OTR Proposal

The purpose of the R&D is to investigate a possible EIC luminosity monitor based on OTR. Backward OTR would measure the total flux of $e^\pm$ pairs that are converted from the bremsstrahlung flux induced by electron-ion collisions. Note that as long as the OTR target is sufficiently downstream of the pair-conversion target that the $e^\pm$ pair has separated by much more than an optical wavelength, there should be no cancellation of radiation. The OTR technique could also be used

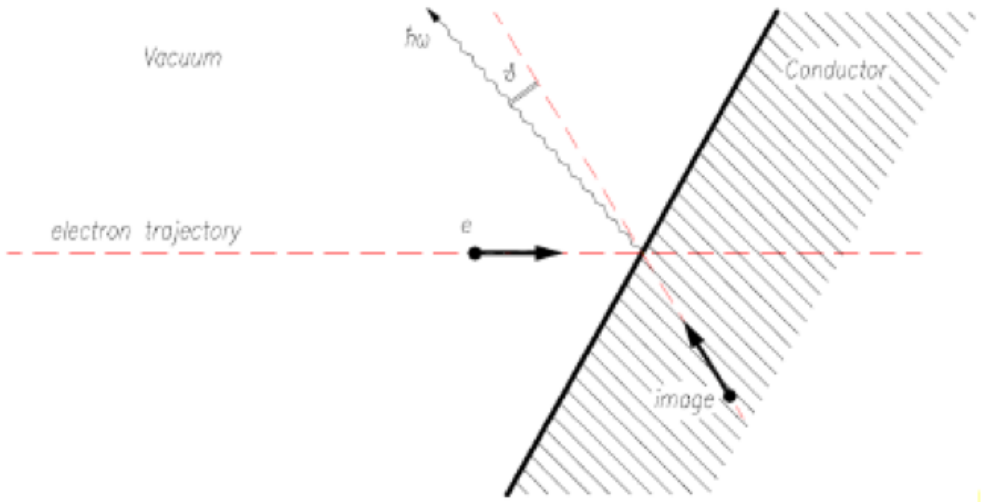

Fig. 8: Optical Transition Radiation (OTR) geometry. Note that the emitted radiation is concentrated around the velocity direction of the image charge, which is also the reflection direction, if the incident electron were instead an optical photon.

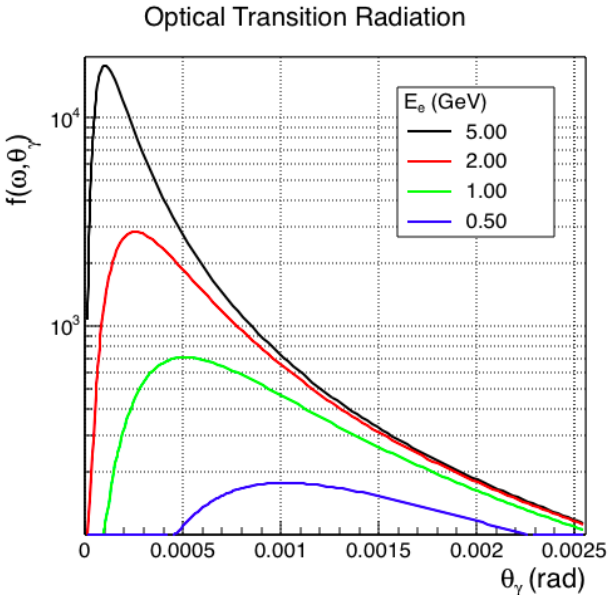

Fig. 9: Optical Transition Radiation flux.

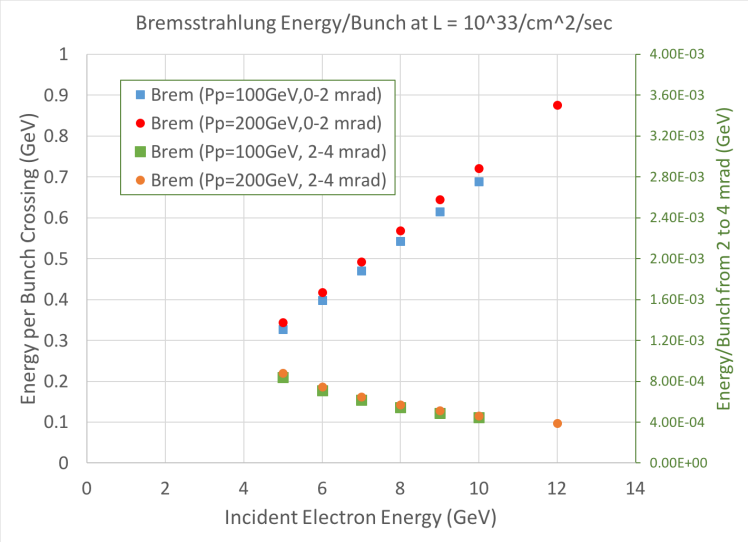

Fig. 10: EIC total bremsstrahlung energy per bunch crossing at a luminosity $\mathcal{L} = 10^{33}/\text{cm}^2/\text{sec}$ and inter-bunch period $T = 2$ nsec. The points are calculated for proton momenta of 100 GeV/c (blue squares) and 200 GeV/c (red circles). The energy integrated from 0 to 2 mrad (detector reference frame) corresponds to the left-hand axis, and the integral values from 2 to 4 mrad correspond to the right-hand axis. Energy per bunch scales with the product $\mathcal{L}T$

to measure a total current of the low Q^2 electrons scattered under very small angles within a fixed solid angle.

ODU graduate student A. Maps calculated the energy and angle dependence of forward bremsstrahlung at the EIC, based on the zero screening limit of the equations of [4]. Her results are summarized in Fig. 10. The bremsstrahlung cone is of order m_e/E, which is much smaller than the *rms* angular spread of the electron beam. However, since the expected beam *rms* is ~ 0.2 mrad, the angular integrals of Fig. 10 should still be accurate. The bremsstrahlung energy spectrum per bunch, expressed as an effective radiation length, it plotted in Fig. 11, for 12 GeV electrons incident on 200 GeV/c protons at a luminosity $\mathcal{L} = 10^{33}/\text{cm}^2/\text{sec}$ and inter-bunch period $T = 2$ ns. The effective radiation length concept means that for photons in a range $k_{\text{Max}} > k_{\text{Min}} > 4$ GeV, the integrated number of photons is

$$N_\gamma \approx 0.06 \log \frac{k_{\text{Max}}}{k_{\text{Min}}} \qquad \text{per bunch crossing.} \tag{6}$$

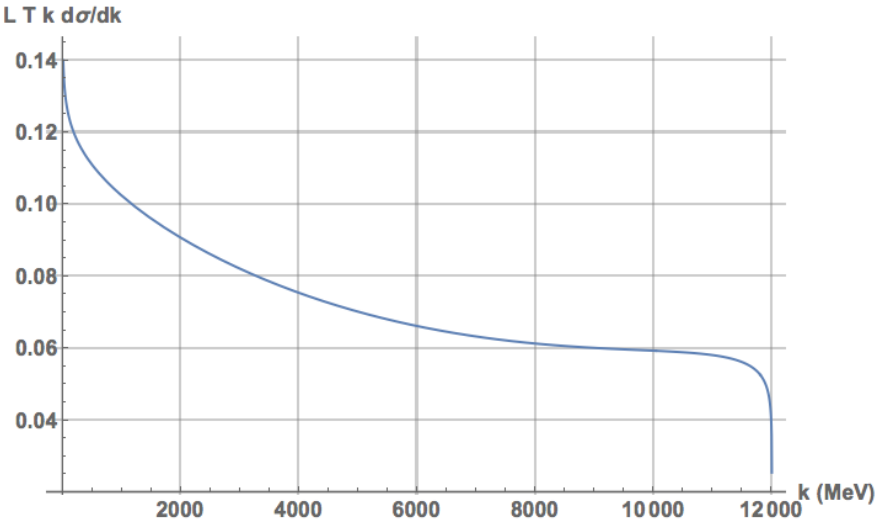

Fig. 11: Energy weighted bremsstrahulung energy spectrum per bunch at a luminosity per bunch $\mathcal{L}T = \left[10^{33}/\text{cm}^2/\text{sec}\right]\left[2\text{nsec}\right]$. The spectrum is calculated for 12 GeV electrons incident on 200 GeV/c protons. The vertical axis is # of photons (see Eq. 6).

Assuming a 1% radiation length pair conversion target, a small flat OTR-mirror can intercept the resulting $e^{\pm}$ (and bremsstrahlung) flux at an arbitrary angle. This mirror should be just large enough to ensure all converted pairs cross it. The photons generated by OTR can be detected by a regular fast photomultiplier tube (PMT). Focussing optics, a Winston Cone concentrator, or an integrating sphere can be used to provide efficient light collection, independent of any variation of the primary electron-ion interaction point, or energy-dependent angular spread of the OTR light. Based on the bremsstrahlung flux (Figs. 10,11) and the OTR yield (Eq. 5 & Fig. 9), we expect to collect 200 to 1000 optical photon (varying with electron beam energy) per sec in an optical band from 350 to 450 nm at $\mathcal{L} = 10^{33}/\text{cm}^2/\text{sec}$. This will yield a 1% measurement of luminosity in 1 minute.

We will study two options for OTR light production and collection:

1. A thin flat OTR radiator installed inside an integrating sphere that has a diameter of ~ 10 inches. This option likely provides the most stable absolute monitor of the OTR flux, and is possibly a candidate for an absolute luminosity monitor. Due to the long collection time of the integrating sphere, this method would not be able to monitor bunch-to-bunch variations in luminosity.

2. An ellipsoidal OTR radiator, with focal length matched to the distance to the PMT. This provides extremely fast response, that can resolve the bunch time-structure. After integration over multiple periods of the beams in the ring, this technique could resolve bunch-to-bunch variations in luminosity.

These two options are illustrated in Fig. 12. Option (1) with an Integrating Sphere was successfully used in the CLAS6 experiments and the corresponding monitor is in storage. There are no doubts about its performance, i.e. regarding its insensitivity on a beam position. The inside surface of the sphere is always covered with some thermoplastic which has a very high (diffusive) reflection coefficient in optical range. But, as any plastic material, it has only limited radiation resistance. It worked very well in JLab Hall B experiments. Option (2) is very radiation resistant both because there are no plastics in use, and because the PMT can be put as far from the beam as space will allow.

Anticipated Outcomes/Results:
We anticipate answering the main question: whether the OTR phenomenon can be used as a fast and precise luminosity monitor in the EIC. Monte-Carlo studies of a realistic design will address issues of light collection, radiation dose, sensitivity to beam parameters (other than luminosity), backgrounds. This will be completed in the first six months of FY2020, leading to the construction and subsequent testing of a prototype. Activities include:

- Monte-Carlo simulations, with priority to light collection.
- Calibration of light detection components
- Tests of the prototype(s) with high energy photon beam. This can be done in the Pair-Spectrometer line of Hall D. This should be done both in vacuo and in air.

Adequate space is available for construction and cosmic ray tests at JLab. The Supplies and Equipment OTR budget is itemized in Table 2. The College of Sciences machine shop at ODU can perform basic machining at no charge to the project. The machining charges in the budget are for high precision items that must be fabricated at JLab.

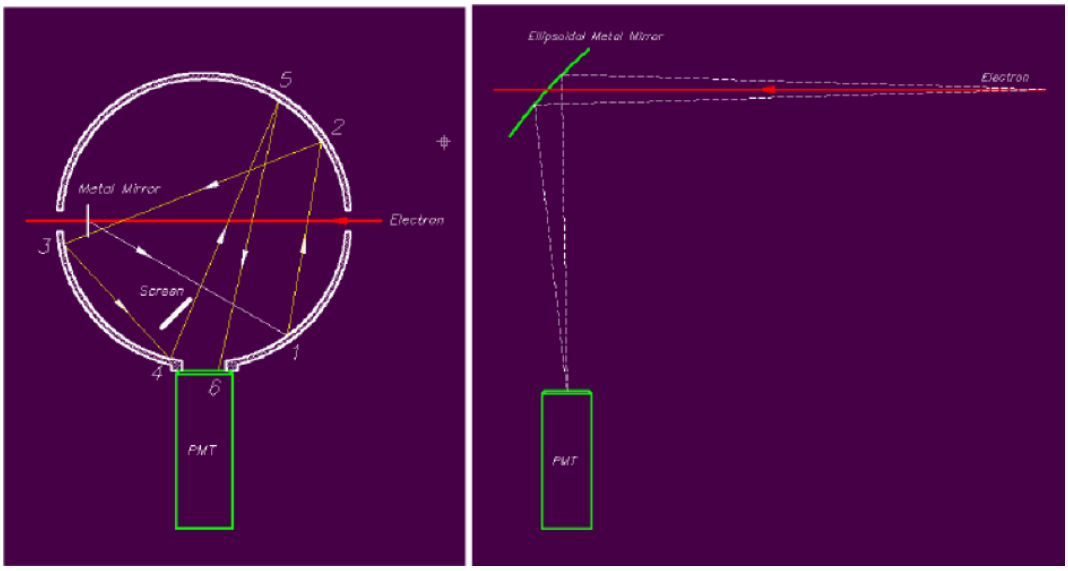

Fig. 12: Two possible configurations for an OTR-based luminosity monitor in the 0° bremsstrahlung line. A thin pair-conversion target would be placed just to the right of either of the figures.

Description	Qty	Unit Cost	Subtotal	Total
Supplies				
Hamamatsu PMT R7724	2	$ 550.	$1100.	
E5859-19 socket and divider	2	$ 419.	$838.	
Magnetic Shield	2	$97.	$194.	
Cables, Connectors, misc.			$1,571.	
Vacuum Components			$2000.	
Supplies Total				$5,707
Machine Shop Charges			$3,226	
Equipment				
Integrating Sphere, 10 in O.D.	1	$7,500	$7,500	
Total (before IDC)				$16,433

Table 2: Supplies and Equipment Budget for OTR Sub-Project. No Indirect Cost (IDC) charges are included. These will be discussed in the Budget Appendix.

References

1. B. Aubert *et al.* (BaBar), Nucl. Instr. Meth. **A479**, 1 (2002), arXiv:hep-ex/0105044 [hep-ex] .

2. V. L. Ginzburg and I. M. Frank, J. Phys.(USSR) **9**, 353 (1945), [Zh. Eksp. Teor. Fiz.16,15(1946)].

3. V. Ginzburg and V. Tsytovich, *Transition Radiation and Transition Scattering* (Taylor and Francis Ltd, 1991).

4. H. W. Koch and J. W. Motz, Rev. Mod. Phys. **31**, 920 (1959).

A Budget

Our proposed FY 2020 budget is described in Table 3.

- Post-Doc salaries plus fringes are charged an off-campus Indirect Cost (IDC) rate of 26%.
- The graduate research assistant (GRA) effort (C. Ploen) is 66% in Spring and 100% in Summer. This salary is charged an on-campus IDC rate of 55% and tuition is charged at $512 per credit hour (exempt from IDC).
- Travel funds are requested to bring M. Sullivan to Jefferson Lab.
- Supplies purchased at ODU (including equipment under $5,000) would be charged the off-campus IDC rate. However, if a different institution has a lower equipment threshold, some items could be reallocated.
- The equipment item (Integrating Sphere) is exempt from IDC.

Person	**Effort**	**Salary**	**Fringes + IDC**	**Total**
PostDocs				
V. Baturin (ODU)	50%	$29,000	$22,156	$51,156
A. Kim (UConn)	50%	$29,000	$22,156	$51,156
GRA				
Ch. Ploen (ODU)	60%	$12,250	$12,997	$25,247
Category		**Cost**	**IDC**	**Total**
Travel (JLab)		$5,000	$2,750	$7,750
Supplies (ODU)		$5,707	$1,484	$7,191
Machine Shop (JLab)		$3,226	$1,774	$5,000
Equipment		$7,500		$7,500
Total				$155,000

Table 3: eRD21 Budget Proposal Summary, FY2020.